ACS OMEGA

http://pubs.acs.org/journal/acsodf

Mini-Review

In Situ TEM of Electrochemical Incidents: Effects of Biasing and Electron Beam on Electrochemistry

Chaoya Han,[†] Md Tariqul Islam,[†] and Chaoying Ni*

Cite This: *ACS Omega* 2021, 6, 6537−6546

Read Online

ACCESS | Metrics & More | Article Recommendations

ABSTRACT: *In situ* TEM utilizing specialized holders and MEMS chips allows the investigation of the interaction, evolution, property, and function of nanostructures and devices responding to designed environments and/or stimuli. This mini-review summarizes the recent progress of *in situ* TEM with a liquid cell and a flow channel for the investigation of interactions among aqueous nanoparticles, electrolytes, and electrodes under the influence of electric bias and electron beam. A focus is made on nanoparticle growth by electrodeposition, particle nucleation induced by electric biasing or electron beam, self-assembly, and electrolyte breakdown. We also outline some future opportunities of *in situ* TEM with aqueous cells and flow.

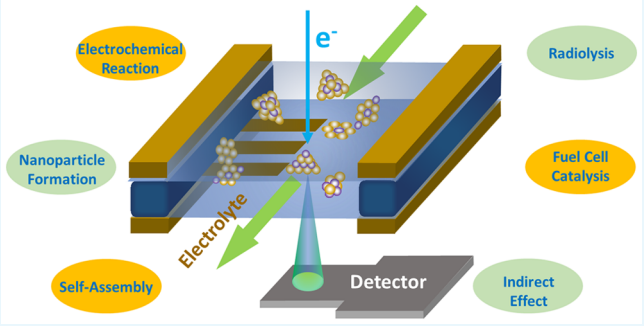

1. INTRODUCTION

In situ experiments involving phase interactions and responses to designed environments afford opportunities for real-time observation, live data acquisition, and specification of reaction dynamics and are often one of the most desirable pathways to explaining some reaction mechanistic fundamentals. Due to its superior spatial resolution down to sub-angstrom resolution and a broad range of associated cutting-edge technological progress in the past few decades, transmission electron microscopy (TEM) has become an indispensable high-end technique in understanding material structures and functions. In parallel, *in situ* TEM utilizing a liquid cell and a flow channel breaks the multiple limits of conventional TEM imposed by the requirement of high vacuum and has been receiving ever-increasing interest in advanced research of materials for energy, environment, and life sciences since its early development.[1,2]

Among various *in situ* TEM results of liquids, one of the most popular themes is on electrochemical reactions related to lithium-ion batteries. Earlier studies focused on the material properties of electrodes and solid electrolytes.[3] With the introduction of a liquid cell, TEM characterization of the interactions at the interface of liquid electrolyte and electrode becomes possible. The liquid cell is also a convenient device for understanding aqueous phase interactions down to the atomic level, such as nanoparticle nucleation, growth, and self-assembly in an aqueous environment.

In this mini-review, we evaluate some recent progress of TEM *in situ* characterization using liquid cells with a focus on a few typical particle−liquid interactions under the influence of an electric field or the incident electron beam.

2. DEVELOPMENT OF *IN SITU* TEM FOR ELECTROCHEMISTRY

2.1. Open Cell for *In Situ* TEM. *In situ* TEM of electrochemistry started with open-cell designs about a decade ago, as shown in Figure 1, where, in addition to the use of electrodes of interest and the significance in battery or fuel cell applications and a miniaturized electric circuit with leads to the outside of the TEM column for the control and measurement of the $I-V$ curve, the selection of liquid electrolytes was limited to ionic liquids simply because an aqueous solution without capsulation would not be compatible with the high vacuum environment in the TEM column and specimen pole pieces required for normal TEM performance. Ionic liquids generally have extremely low vapor pressures even at elevated temperatures or as exposed to high-energy electron beam irradiation and thus can provide a transport path for ions and electrons between the electrodes in TEM. In 2011, Liu and Huang proposed nano lithium-ion battery designs for TEM experiments,[4] representing the pioneering efforts on modern *in situ* TEM of electrochemistry and the direct observation of electrochemical interactions among charge species, electrodes, and electrolytes. They also utilized Li_2O as a solid electrolyte.

Received: December 1, 2020
Accepted: February 18, 2021
Published: March 2, 2021

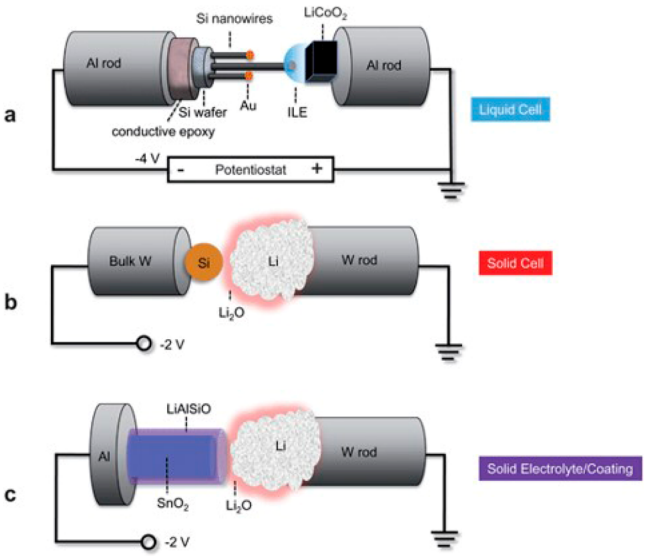

Figure 1. Schematics of open-cell lithium-ion batteries designed for TEM observation. (a) Liquid cell with ionic liquid electrolytes (ILE). (b) Solid cell with Li_2O as the solid electrolyte. (c) Solid cell with more layers serving as electrolytes.[4] The figure is adapted with permission from ref 4. Copyright 2011 Royal Society of Chemistry.

The open-cell design has the advantage of relatively simple setup, easy handling, and high compatibility with the TEM column vacuum environment. However, the most common and important electrochemical reactions involve aqueous electrolytes instead of ionic liquids. The challenge has inspired significant and continuous efforts on the TEM of electrochemistry, including the development and fabrication of special holders and disposable chips to allow the observation and characterization of chemical and electrochemical interactions in aqueous solutions.

2.2. Sealed Liquid Cells. In hindsight, the concept of a sealed cell for TEM can be traced back to the 1960s. In 1962, Heide reported a sealed-cell design under a controllable gas environment (other than vacuum) and its potential applications in biology.[5] A milestone was reached in 2003 by Ross *et al.*, who designed and fabricated a liquid cell, as shown in Figure 2, leading to a ground-breaking TEM characterization of electrochemical interactions.[6]

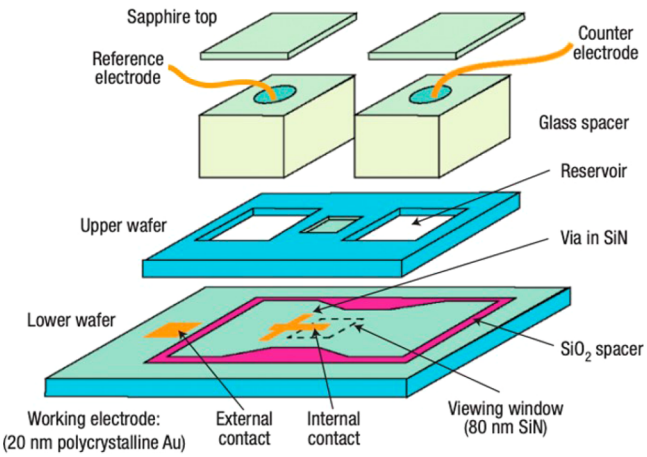

Figure 2. Schematic of the sealed liquid cell.[6] The figure is adapted with permission from ref 6. Copyright 2003 Springer Nature Limited.

The closed-cell design consists of two silicon wafers with a Si_3N_4 viewing window in the middle on each of them aligned with each other for electron beam penetration and observation. Between the two wafers, a thin SiO_2 layer (red rectangular band in Figure 2) serves as a spacer and also for the realization of a closed cell by sealing the spacer. The liquid electrolyte is injected with a syringe into a reservoir right before the experiment. The electrolyte then flows by capillary action, passes between the double-layer Si_3N_4 viewing window across which a predeposited Au nanowire working electrode connects to a power supply through the "internal contact" in the sketch, and reaches another reservoir on the other side of the viewing window. The closed liquid cell setup offers a device to directly record the electrochemical interactions.

Despite the breakthrough in liquid cell design, only a very limited image resolution was initially achievable. The thickness of the viewing window immediately became crucial for resolution improvement. In 2009, Zheng *et al.* used a liquid cell design with 25 nm silicon nitride windows and reported a sub-nanometer resolution.[1] However, decreasing the thickness of the viewing window could also risk the reliability of performance of the sealed cell. It is also important to balance the window size and the cell thickness to ensure a good resolution with sufficient field of view and adequate cell volume for typical material interactions to occur simulating a real world environment. Even though silicon nitride has been dominating the material choice for the viewing window, in 2012, Yuk *et al.* reported a sealed liquid cell design with layers of graphene, and it led to significant resolution improvement compared to that of other liquid cell designs due to considerably decreased scattering occurrences in the ultrathin graphene layers wrapping around the liquid to be observed.[8]

While fully sealed liquid cells were initially employed for the observation of a static environment and remain an option for many TEM observations, tracking a liquid flow and interactions within it has been quickly recognized to be the most desirable in many circumstances. For example, in 2009, de Jonge *et al.* imaged whole eukaryotic cells in liquid using a flow cell design of silicon nitride windows.[7] In early 2020, Dunn *et al.* reported a graphene-sealed flow cell with better performance in achieving high resolution.[8]

The initial customized lab-scale setups clearly demonstrated the feasibility and potential of *in situ* TEM with miniature devices achievable by a route of modern nanofabrication for unprecedented TEM results and insights into chemical and electrochemical reactions. Robust development efforts on commercial products have been made by Protochips,[9] Hummingbird Scientific,[10] DENSsolutions,[11] Bruker,[12] Gatan,[13] and a few others, which promise a broad range of opportunities for the high-resolution *in situ* characterization of physical and chemical occurrences and dynamics in designed environments and stimuli.

2.3. Advantages of *In Situ* TEM over Other *In Situ* Methods. The major advantages of TEM over other imaging methods are well summarized in Figure 3, one of which is the high spatial resolution down to sub-angstrom. Another relatively less known advantage is the high temporal resolution.[14] The limiting factor of TEM temporal resolution is often only related to recording, which is further being dramatically improved as the digital imaging and recording technology breakthroughs continue.

While the high spatial resolution of TEM can generally be retained for most *in situ* observations involving heating and

https://dx.doi.org/10.1021/acsomega.0c05829
ACS Omega 2021, 6, 6537−6546

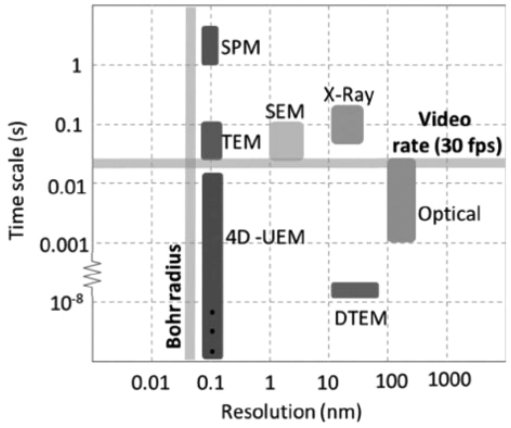

Figure 3. Resolution of microscopic methods, including TEM techniques, DTEM (dynamic TEM), 4D-UEM (four-dimensional ultrafast electron microscopy).[14] The figure is adapted with permission from ref 14. Copyright 2012 Wiley-VCH Verlag GmbH & Co. KGaA, Weinheim.

mechanical force, the liquid environment and liquid cell capsulation can compromise the TEM detection limit. Many efforts have been made to improve capsulation materials and the design and control of aqueous flow and pumping systems, among many other challenges and opportunities.[15] The steady progress in TEM holder and accessories has enabled the *in situ* TEM technique to have better and expanded control of experimental conditions. For example, in 2015, Leenheer *et al.* designed a sealed liquid cell with the chips and accessories being capable of controlling electrochemical conditions to have a picoampere level precision.[16] Most of the flow cell designs and many corresponding commercial products mentioned in previous sections can control the liquid flow as well, and some of them can also achieve temperature control. A broadening selectivity of the sealed cells available from commercial sectors affords the precise control of various electrochemical conditions, and such capacity is bringing growing advantages over other *in situ* methods.

3. ELECTROCHEMICAL REACTIONS IN LIQUID CELLS WITH ELECTRIC BIAS

In situ TEM of electrochemistry provides essential and unprecedented opportunities for the understanding of electrochemical interactions in lithium-ion batteries or fuel cells.[17−19] This section summarizes a few selected liquid-cell electrochemistry studies. The electron beam (also termed as e-beam) effects and e-beam induced incidents are also discussed.

3.1. Electrodeposition. Electrodeposition and its reverse process, electropolishing, have extensive applications in industrial-scale processes and fabrications such as those in the manufacturing of tools, machine parts, and semiconductor devices. The phenomena also occur at the interface of electrolyte and electrodes in batteries and fuel cells,[20,21] oftentimes coupled with desirable and undesirable consequences. An internal short circuit due to electrodeposition and growth at the electrodes is a classical example of the main causes leading to a catastrophic breakdown of battery or fuel cell devices. Chen *et al.* used a sealed liquid cell to observe the nickel electrodeposition and the electropolishing when a reversed biasing was applied to switch for the etching.[20] The experiment reveals some fundamentals about how the metal nanostructures form and grow at a solid−liquid interface and how they dissolve, as shown in Figure 4, in which panels a−f record the dynamic interactions of electrodeposition and electropolishing. Panels a−c indicate that the nickel dendrites grow at different rates: the rate at stem tip is higher than that of the dendrites in between the stems. The nonlinear solid−liquid interface movement suggests that both of the solution composition and the local field can influence the deposition process. The deposition can sustain for a short period of time

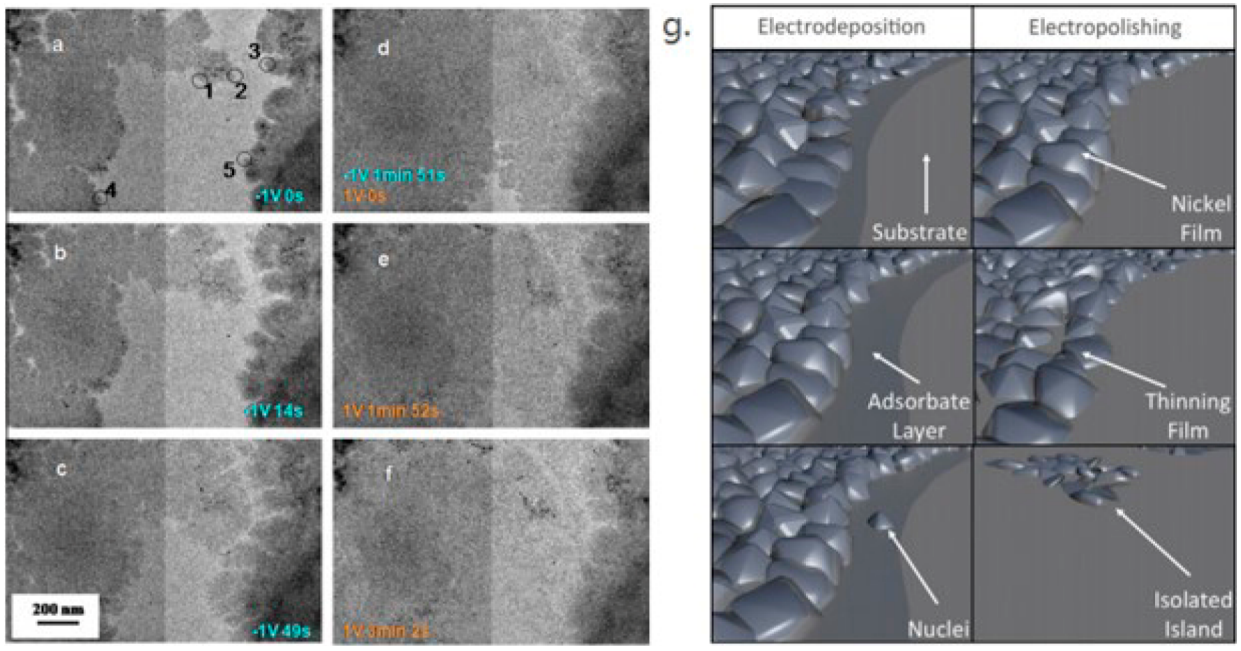

Figure 4. (a−c) *In situ* TEM images of nickel electrodeposition at a bias of −1 V. (d−f) *In situ* TEM images of nickel electropolishing at a bias of 1 V. (g) Proposed mechanisms of electrodeposition and electropolishing.[20] Panels a−g are adapted with permission from ref 20. Copyright 2012 Acta Materialia Inc. Published by Elsevier Ltd. All rights reserved.

https://dx.doi.org/10.1021/acsomega.0c05829
ACS Omega 2021, 6, 6537−6546

after the bias is turned off. In contrast to the electrodeposition, the electropolishing at reversed biasing etches the dendritic deposits at a uniform rate, and the deposits eventually break down into islands before they dissolve completely. Based on these observations, Figure 4g proposes that an adsorbate layer forms during the electrodeposition on which the nickel nanoparticles nucleate heterogeneously and grow. Stepwise, the electropolishing preferentially breaks the film followed by the formation of islands and the dissolution of nanoparticles.

A similar *in situ* TEM study was conducted by Sacci *et al.* in 2014 for the investigation of lithium deposition and dendritic growth to achieve safe, more efficient, and longer lifetime lithium-ion batteries.[21] This study concludes that a compound dendritic structure starts to grow before the lithium deposition, and the latter can occur within the SEI (solid electrolyte interface) layer in addition to those formed outside, as shown in Figure 5.

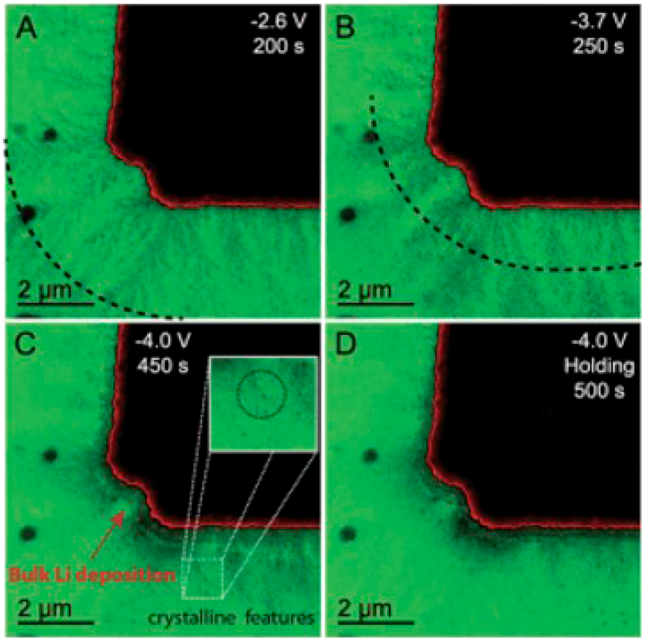

Figure 5. Frames captured under different conditions and formation of SEI layers.[21] Panels A–D are adapted with permission from ref 21. Copyright 2014 Royal Society of Chemistry.

3.2. Fuel Cell Catalysis. Catalysts play an indispensable role in modern fuel cells. Understanding how the catalyst interacts with reactants is critical in the study of fuel cells. With the development of liquid cell chips, *in situ* TEM has become a favorite choice of characterization technique for discoveries in fuel cell research. Using this technique, Beermann *et al.* studied the degradation of a Pt–Ni alloy catalyst supported on carbon under electrical biasing.[22] They employed a sealed liquid cell with a viewing window for STEM (scanning transmission electron microscopy) observation and characterization. Figure 6 shows the structural evolution of the catalyst at a time sequence and electrical potential cycle. By the real-time observation and recording, the alloy catalyst degradation reactions of $Ni^0 \rightarrow Ni^{2+} + 2e^-$ and $Pt^0 \rightarrow Pt^{2+} + 2e^-$ were found to occur corresponding to different electrical potentials. The *in situ* study also identified a preferential growth trend of Pt/Ni alloy particles, and the aggregation of these particles favors the octahedral facets. By correlating the cycling voltage with catalyst degradation, an optimal working voltage was therefore proposed for better sustainability.[16] This research broke new ground in the high-resolution visualization of microscale fuel cell catalysis. The observations helped provide a broad understanding of the activation and degradation of alloys with different compositions, the corrosion of support materials, and the importance of controlling electrochemical conditions. This type of research further paves the way for the study of fuel cell catalysis to elucidate reaction mechanisms in nanoscale and atomic resolution.

4. ELECTRON BEAM INCIDENTS

TEM operates in significant kiloelectronvolt ranges that could trigger side reactions and affect image formation. Incidents like elastic (electron–nucleus) scattering and inelastic scattering could happen due to the application of an e-beam. These two types of scattering can have two different consequences while interacting with the sample media. Elastic scattering could lead to atomic displacement and e-beam sputtering and redeposition. On the other hand, specimen heating, contamination, and other damages or energy transfer could be consequences of inelastic scattering.[23] Therefore, using TEM to observe materials in a liquid cell has additional challenges. The effect of the electron beam needs to be considered in advance.

The beam effect on materials is a function of incident electron energy of the beam, dose rate, *e.g.*, $e^-/(s\cdot Å^2)$, and beam diameter. Materials are susceptible to specific beam parameters depending on their composition, atomic structure, and the local environment. The main effects of an electron beam with the electrolyte can be understood in an electron–electrolyte interaction framework,[24] which can be termed as a direct effect. Some indirect effects (*i.e.*, secondary effects) of the beam include beam-induced nanoparticle growth, lithiation, displacement of fluid/atom, electrolyte breakdown, bubble formation, and nanoparticle precipitation/dissolution in the electrolyte, to name a few.

4.1. Radiolysis of Liquid and Applications in *In Situ* TEM Studies. After the electron irradiation on water with electron beam energy (keV) higher than a threshold, there will be aqueous electrons in the water.[24] The primary reactions and their products are shown below:[24]

$$H_2O \rightarrow e_{aq}^-, H^\bullet, OH^\bullet, HO_2^\bullet, OH^-, H_3O^+, H_2, H_2O_2 \quad (1)$$

These newly introduced species could influence the experiment and should often be considered before the experiment. On the other hand, for *in situ* TEM studies, there are times when radiolysis of water could be used on purpose.

In 2020, Huang *et al.* reported a study on using the e-beam to retrieve Li from LiF.[25] Of many lithium salts that are used in Li-ion batteries, $LiPF_6$ has shown high potential. However, its chemical instability poses some real problems. $LiPF_6$ degrades easily, forming LiF, and such degradation results in capacity fading and a failed device. The equilibrium reaction $LiPF_6 \rightarrow LiF(s) + PF_5(g)$ goes to the right if the gaseous product, PF_5, is released into the environment, left with LiF solid to shorten the life cycle of the energy device.

In their experiment, e-beam irradiation causes inelastic-scattering-induced radiolysis, and thus alkali halides (*i.e.*, LiF) produce short-lived double-halogen ions (H-center) and an anion vacancy (F-center). These defects also aggregate themselves, diffuse to the surface, cause the loss of halogen atoms, and liberate the alkali metals in the process.

https://dx.doi.org/10.1021/acsomega.0c05829
ACS Omega 2021, 6, 6537–6546

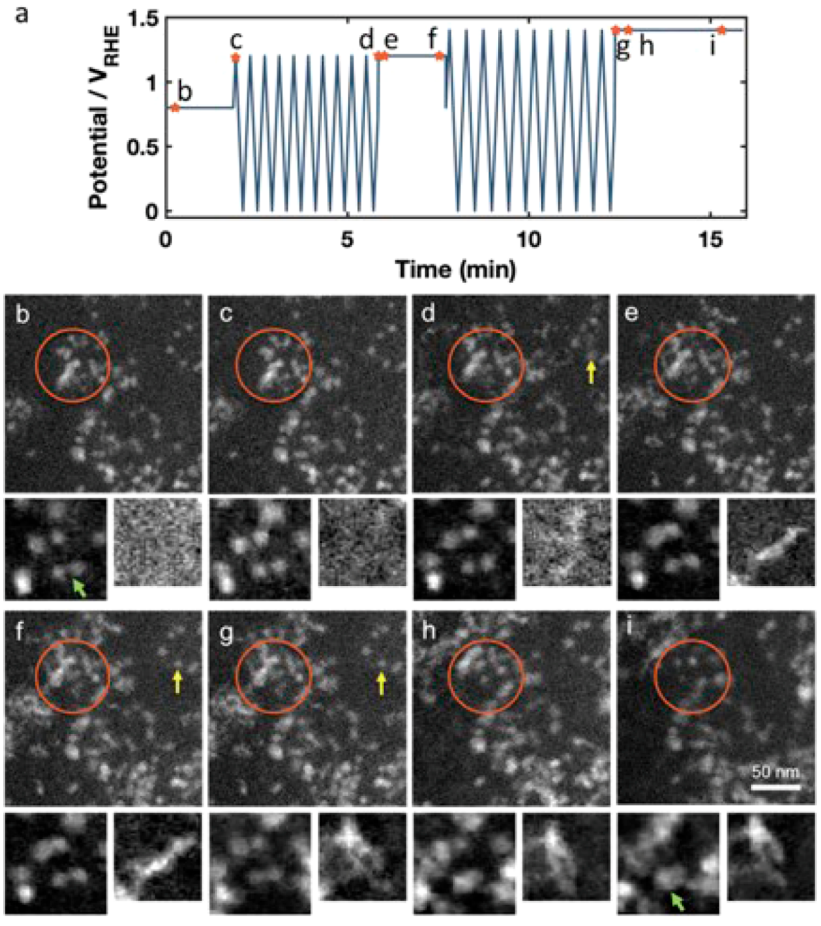

Figure 6. High-angle annular dark-field STEM images of catalyst structure change over electrochemical potential cycling. (a) Applied potential over time. (b–i) STEM images of catalyst structure change labeled on (a) at their corresponding time and electrical potential.[22] Panels a–i are adapted with permission from ref 22. Copyright 2019 Royal Society of Chemistry.

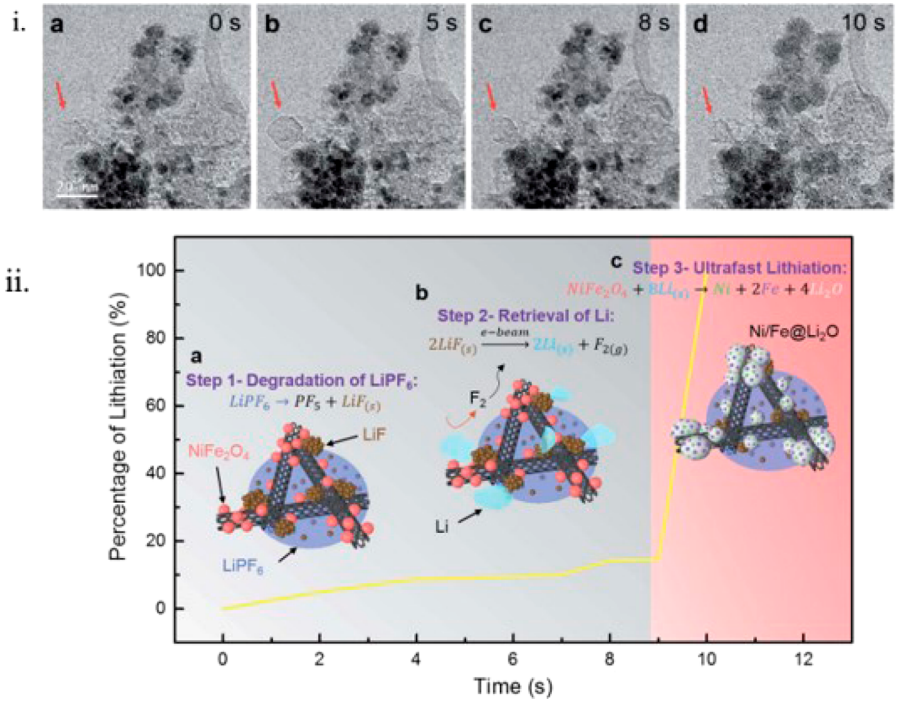

Figure 7. (i) TEM images of lithiation, nanoparticles, and nanoparticle accumulation into clusters. (ii) Schematic of the reactions.[25] Panels i and ii are adapted with permission from ref 25. Copyright 2020 Royal Society of Chemistry.

https://dx.doi.org/10.1021/acsomega.0c05829
ACS Omega 2021, 6, 6537–6546

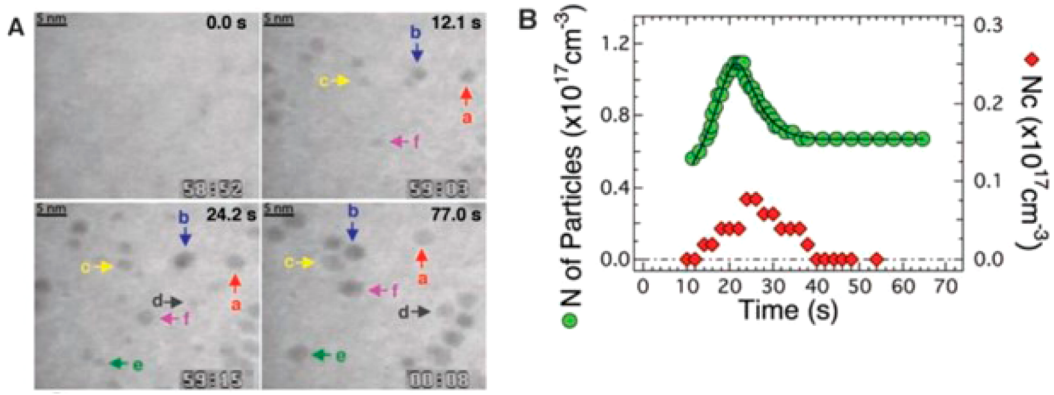

Figure 8. Growth and coalescence of Pt nanocrystals. In (A), specific particles are marked with arrows depicting the growth trajectories as a function of time while being subjected to the electron beam. In (B), the number of particles (left axis) and the number of coalescence events (Nc, right axis) are presented along with time. Particles nucleate and grow while being observed.[1] Panels A and B are adapted with permission from ref 1. Copyright 2009 American Association for the Advancement of Science.

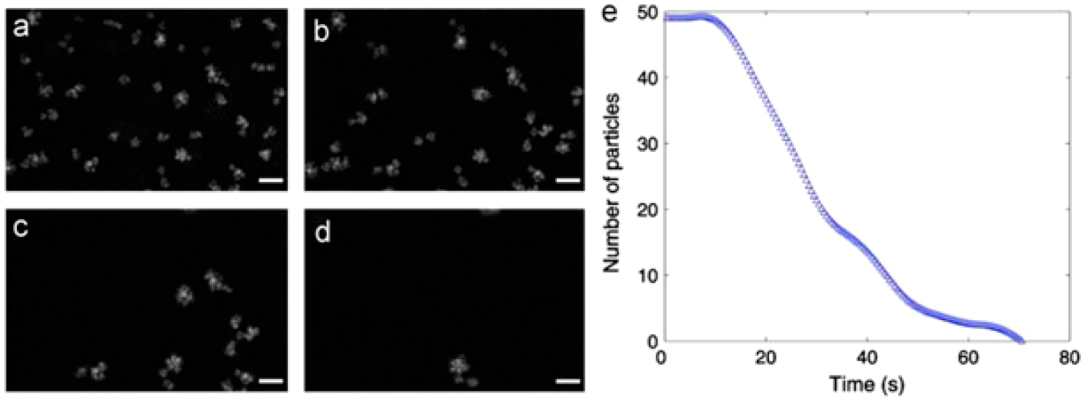

Figure 9. Series of high-angle annular dark-field STEM images of TiO_2 aggregates which are expelled from the view area at (a) t = 0 s, (b) t = 20 s, (c) t = 40 s, and (d) t = 60 s. (e) Number of aggregates as a function of time during 75 s of electron irradiation. M = 300,000, the electron dose rate is 10 $e^-/(s{\cdot}A^2)$, and the scale bars are 50 nm.[24] Panels a–e are adapted with permission from ref 24. Copyright 2013 Elsevier B.V. All rights reserved.

They also observed, as shown in Figure 7, that $LiPF_6$ degrades and LiF clusters precipitate on the $NiFe_2O_4$/carbon nanotube electrode material. After e-beam irradiation, the radiolysis of LiF follows the reaction $2LiF \rightarrow 2Li + F_2$, which relieves the negative effect of $LiPF_6$ ionic liquid electrolyte degradation, liberating Li. LiF acts as a Li source for ultrafast chemical lithiation of an electrode material, such as $NiFe_2O_4$/carbon nanotubes.

4.2. Electron-Beam-Induced Nanoparticle Growth. Nanoparticles may form and grow when exposed to electron beams, and that can be a function of time (see Figure 8B).[1] The growth initiates in the Pt^{2+} precursor solution, and nanocrystals emerge. What appears special here is that the particle growth and the nucleation occur in parallel instead of sequentially as often seen in classical solidification (particles marked in Figure 8A, showing a growth trend). Particles grow conventionally by monomer addition from the solution, and coalescence happens between the particles. The number of particles increased during the beginning of the growth stage and then reached a maximum. A significant decrease in particles was then observed, which reached a constant value further in the process. Some particles tend to dissolve, contributing to the decrement of particles here, but the particle coalescence could explain the main reason for the decreased number as the TEM beam time continues (coalescence events in Figure 8B).

The electron beam can significantly interact with free nanoparticles in suspension, as shown in Figure 9 by Woehl *et al.*[24] As time progresses, individual TiO_2 particle clusters grow, and a significant portion of the clusters are repelled from the area of interest suddenly, moving perpendicular to the optical axis (direction of unreflected electron beam). Aggregates apparently can be moving faster than STEM's time resolution of the scan, and for that reason, the particles are not seen leaving the viewing area. In Figure 9e, the initial number of particles (N of particles) is fixed until 10 s. That suggests a time frame of the charging-related phenomenon acquired from the incident electron beam by the particles, and later these particles are subjected to repulsion. When the high-energy electron beam hits the liquid, a large amount of energy is transmitted through the sample, creating charge imbalance in the sample and therefore charging the particles to a point that causes the particle repulsion.

4.3. Electron-Beam-Induced Self-Assembly. Liu *et al.* documented a process of self-assembly of gold nanoparticles in solution after the nanoparticles were coated by positively charged cetyltrimethylammonium ions (CTA^+) or negatively charged citrate ions (Cl^-).[26] The nanoparticles with CTA^+ were observed to form a one-dimensional structure after the e-

https://dx.doi.org/10.1021/acsomega.0c05829
ACS Omega 2021, 6, 6537–6546

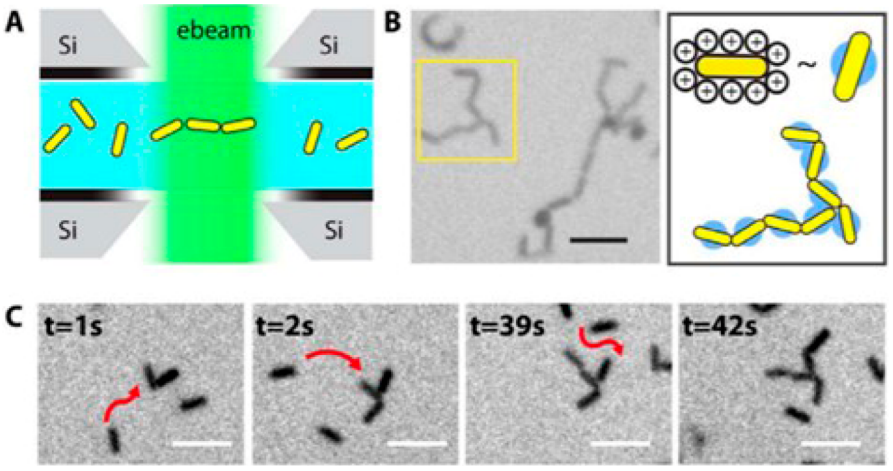

Figure 10. Tip-to-tip assembly of Au nanorods by *in situ* liquid-phase TEM. (A) Typical *in situ* liquid TEM setup with Si_3N_4 windowed microchips. Due to the application of the e-beam, well-dispersed Au nanorods self-assemble. (B) Respective TEM image (left) and schematics (right) depicting the final assembled structures. (C) Time series of TEM images demonstrating the approach and attachment mechanism of Au nanorods. The trajectories are indicated by red arrows that show incidents before the nanorods' attachment to each other to form clusters and grow the rod assemblies. The scale bar is 100 nm.[27] Panels A–C are adapted from ref 27. Copyright 2015 American Chemical Society.

beam irradiation due to a decreased repulsive force between the nanoparticles. However, the nanoparticles with Cl^- coating did not respond to each other no matter how the beam dose was changed. Later Chen *et al.* reported a similar work on *in situ* TEM experiment to show the self-assembly of gold nanorods after e-beam irradiation in a liquid cell.[27] The occurrence of nanorod assembly was found to be dependent on an anisotropic interaction potential, which is a strong function of the liquid environment (*i.e.*, ionic strength). The anisotropic interaction potential could then be extracted by TEM observation of the pairwise interaction between nanocrystals. As illustrated in Figure 10, this anisotropic interaction potential directs the Au nanorods to attach themselves in a selective tip-to-tip fashion within the liquid due to a long-range and highly anisotropic electrostatic repulsion.

Similarly, organic nanoparticles can be manipulated by the e-beam to assemble into clustered structures, as reported by Zheng *et al.*[28] Under the influence of electron beam, diblock copolymers were observed to form spherical micelles and other nanostructures in solution.[29]

We suspect that the technique of electron-beam-assisted assembly of nanostructures enabled by TEM will have increased application in research and even in device fabrications.

4.4. Other Electron Beam Effects. *4.4.1. Bubble Formation.* Klein *et al.*[30] revealed that intense electron irradiation when the beam was converged by a condenser lens could displace fluid in liquid by a gas phase, resulting in a highly distorted image (Figure 11c). Understandably, the water can vaporize as the intensely focused electron beam deposits sufficient energy locally. Additionally, the hydrolysis of water could be another cause of the bubble. The electron-beam-induced turbulence in the liquid can extend to the surrounding areas relative to the beam position, generating fluid expulsion from the TEM field of view. In Figure 11, images (a) and (b) record the features in the viewing area when a relatively low dose average rate is used, whereas image (c) is acquired when an intense dose rate is applied. Image (d) has the same field of view as that of image (c) but is collected at a normal electron dose rate.

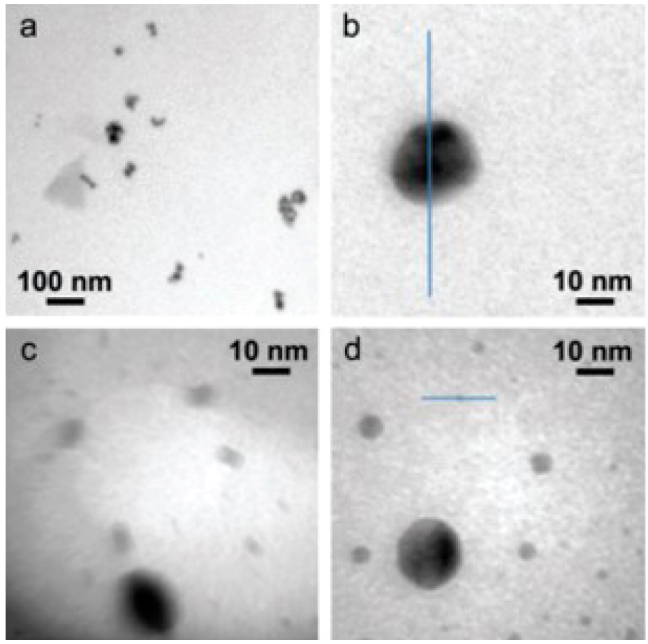

Figure 11. TEM bright-field images and inverted intensity line profiles of gold nanoparticles positioned within the microfluidic cell at the beam exit surface. (a) Lower magnification shows the presence of different sized clusters of nanoparticles. (b) Higher magnification shows an individual nanoparticle with a 20 nm diameter. (c) Image acquired during high e-dosage and incident of e-beam-induced partial displacement of the fluid. (d) Image of the same region in (c) depicting the displacement of the fluid.[30] Panels a–d are adapted with permission from ref 30. Copyright 2011 John Wiley and Sons.

4.4.2. Lowering of the Electrochemical Potential. Electron beam irradiation can also lead to the lowering of the electrochemical potential of specimens, as reported by Hodnik *et al.*[31] For Pt-based nanocatalysts subjected to potential cycling, the degradation mechanisms usually include catalyst particle agglomeration and dissolution, which may lead to the detachment of catalytic components from the electrode. After multiple potential cycles, abnormal growth of the Pt catalyst was observed by *in situ* TEM with a liquid cell, as shown in

https://dx.doi.org/10.1021/acsomega.0c05829
ACS Omega 2021, 6, 6537–6546

Figure 12, where the PtCu/C electrocatalyst was detached and then negatively charged due to the e-beam. Additional growth

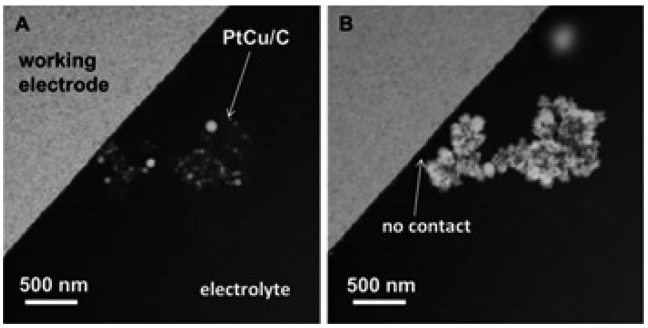

Figure 12. Electrochemical *in situ* liquid cell TEM images of PtCu/C electrocatalysts before (A) and after (B) 150 potential cycles at 0.5 V/s in 0.1 M $HClO_4$.[31] Panels A and B are adapted from ref 31. Copyright 2016 American Chemical Society.

of the detached Pt nanoparticles was observed due to Pt diffusion from the electrode *via* solution on further electrochemical cycling, suggesting a potential lowering of the catalysts. The rest of the particles which were still attached to the electrode did not show this type of phenomenon.

5. SUMMARY AND OUTLOOK

The past couple of decades have witnessed remarkable progresses in *in situ* TEM, including a broad range of applications of the techniques for the characterization of phase interactions in liquids with specialized holders and MEMS chips. As manifested by some selected examples discussed in previous sections, the liquid cell *in situ* TEM is indeed a powerful technique for the characterization of phase behavior in solution, particle−particle interaction, self-assembly, and the electrochemical interactions simulating an environment in batteries or fuel cells, such as electrolyte−electrode interactions, phase transformation in electrodes, and dendritic growth at the interface of the electrode−electrolyte. In most *in situ* TEM experiments, the electron beam of adequate dose and energy has negligible or limited negative impacts on the experimental results. There are also times when the electron beam can be favorably utilized as a desired participating component for a phenomenon or reaction to occur. However, the high-energy electron beam is a factor that may introduce undesirable side reactions, artifacts, and damages to the specimens and devices. To minimize such unfavorable impacts, using low-dose electron beam, cryogenic holder, or pole-piece cryo-box, together with high sensitivity camera, is already a trend of the technological development. There are also significant efforts in commercial laboratories on the development of more user-friendly holders, chips, and liquid pumping systems for better control of the experiment parameters and less detrimental beam effects. More recently, advanced computer software−instrument interfacing, artificial intelligence, and machine learning have increasingly been recognized and developed to play roles in TEM for automated and efficient operation, parameter optimization, image acquisition, and data processing. These developments obviously are especially beneficial for liquid-phase *in situ* TEM.

AUTHOR INFORMATION

Corresponding Author

Chaoying Ni − *Department of Materials Science and Engineering, University of Delaware, Newark, Delaware 19716, United States;* orcid.org/0000-0001-6043-508X; Email: cni@udel.edu

Authors

Chaoya Han − *Department of Materials Science and Engineering, University of Delaware, Newark, Delaware 19716, United States;* orcid.org/0000-0003-2234-5969

Md Tariqul Islam − *Department of Materials Science and Engineering, University of Delaware, Newark, Delaware 19716, United States*

Complete contact information is available at: https://pubs.acs.org/10.1021/acsomega.0c05829

Author Contributions

†C.H. and M.T.I. contributed equally.

Notes

The authors declare no competing financial interest.

Biographies

Chaoya Han received his Bachelor of Science degree from the University of California, Los Angeles (UCLA), in 2016. He then earned his Master of Science degree from the University of Illinois at Urbana—Champaign (UIUC) in 2018. In 2019, he joined the University of Delaware and became a Research Assistant in Dr. Chaoying Ni's group. His research focuses on laser-induced damage on ceramics and *in situ* TEM in electrical and electrochemical reactions.

Md Tariqul Islam is from Dhaka, Bangladesh. After completing his B.Sc. degree from the Department of Materials and Metallurgical

https://dx.doi.org/10.1021/acsomega.0c05829
ACS Omega 2021, 6, 6537−6546

Engineering at Bangladesh University of Engineering and Technology (BUET) in 2017, he joined the Department of Materials Science and Engineering at the University of Delaware as a Research Assistant in 2019 to pursue his Ph.D. under the supervision of Dr. Chaoying Ni. His research interests include *in situ* electron microscopy, *in situ* electrochemistry, and energy conversion.

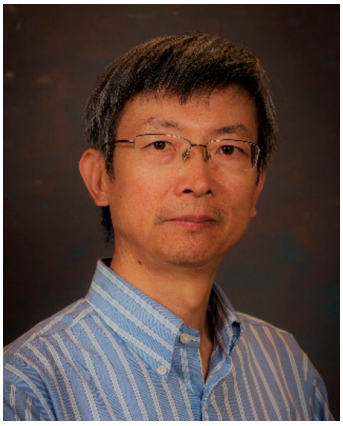

Chaoying Ni is a Professor in the Department of Materials Science and Engineering and has also been serving as the Director of the W. M. Keck Center for Advanced Microscopy and Microanalysis at the University of Delaware since the founding of the center in 2001. He received a Ph.D. degree in Materials Science from the University of Delaware, followed by a short stay of postdoctoral research in physics on the campus before leaving for industrial positions. His previous professional experiences include a stint of a few years as scientist and metrologist in environmental industry and a corporation of semiconductor manufacturing and specialty chemicals in the U.S. in addition to a number of earlier years in China on the faculty of Jiangnan University and as a researcher in the railway industry and the China Academy of Railway Sciences. His research interest centers on the correlation of processing, structure and property of novel material nanostructures and composites, transmission electron microscopy and scanning electron microscopy, high-resolution *in situ* and operando techniques, with expertise including electron crystallography and e-beam associated spectroscopy. His active efforts are on advanced composites, materials for energy and environment, mesoporous crystals, functional nanostructures and assemblies, thin films, interfaces, and coherent growths. He has published over 200 journal papers, a number of book chapters and patents.

■ ACKNOWLEDGMENTS

The authors gratefully acknowledge the partial support from II–VI Foundation.

■ REFERENCES

(1) Zheng, H.; Smith, R. K.; Jun, Y.-w.; Kisielowski, C.; Dahmen, U.; Alivisatos, A. P. Observation of single colloidal platinum nanocrystal growth trajectories. *Science* **2009**, *324* (5932), 1309–1312.
(2) De Jonge, N.; Ross, F. M. Electron microscopy of specimens in liquid. *Nat. Nanotechnol.* **2011**, *6* (11), 695–704.
(3) Armstrong, M. J.; O'Dwyer, C.; Macklin, W. J.; Holmes, J. D. Evaluating the performance of nanostructured materials as lithium-ion battery electrodes. *Nano Res.* **2014**, *7* (1), 1–62.
(4) Liu, X. H.; Huang, J. Y. In situ TEM electrochemistry of anode materials in lithium ion batteries. *Energy Environ. Sci.* **2011**, *4* (10), 3844–3860.
(5) Heide, H. G. Electron microscopic observation of specimens under controlled gas pressure. *J. Cell Biol.* **1962**, *13* (1), 147–152.
(6) Williamson, M.; Tromp, R.; Vereecken, P.; Hull, R.; Ross, F. Dynamic microscopy of nanoscale cluster growth at the solid-liquid interface. *Nat. Mater.* **2003**, *2* (8), 532–536.
(7) de Jonge, N.; Peckys, D. B.; Kremers, G.; Piston, D. Electron microscopy of whole cells in liquid with nanometer resolution. *Proc. Natl. Acad. Sci. U. S. A.* **2009**, *106* (7), 2159–2164.
(8) Dunn, G.; Adiga, V. P.; Pham, T.; Bryant, C.; Horton-Bailey, D. J.; Belling, J. N.; LaFrance, B.; Jackson, J. A.; Barzegar, H. R.; Yuk, J. M.; Aloni, S.; Crommie, M. F.; Zettl, A. Graphene-Sealed Flow Cells for In Situ Transmission Electron Microscopy of Liquid Samples. *ACS Nano* **2020**, *14* (8), 9637–9643.
(9) Protochips. *In Situ* TEM Solutions. https://www.protochips.com/products/ (accessed November 30, 2020).
(10) Hummingbird Scientific. http://hummingbirdscientific.com/ (accessed November 30, 2020).
(11) DENSsolutions. https://denssolutions.com/ (accessed November 30, 2020).
(12) Bruker. Hysitron PI 95 TEM PicoIndenter. https://www.bruker.com/products/surface-and-dimensional-analysis/nanomechanical-test-instruments/nanomechanical-test-instruments-for-microscopes/pi-95-tem-picoindenter/overview.html (accessed November 30, 2020).
(13) Gatan. https://www.gatan.com/ (accessed November 30, 2020).
(14) Espinosa, H. D.; Bernal, R. A.; Filleter, T. In situ TEM electromechanical testing of nanowires and nanotubes. *Small* **2012**, *8* (21), 3233–3252.
(15) Xie, Z.-H.; Jiang, Z.; Zhang, X. Promises and challenges of in situ transmission electron microscopy electrochemical techniques in the studies of lithium ion batteries. *J. Electrochem. Soc.* **2017**, *164* (9), A2110.
(16) Leenheer, A. J.; Sullivan, J. P.; Shaw, M. J.; Harris, C. T. A sealed liquid cell for in situ transmission electron microscopy of controlled electrochemical processes. *J. Microelectromech. Syst.* **2015**, *24* (4), 1061–1068.
(17) Zeng, Z.; Liang, W.-I.; Liao, H.-G.; Xin, H. L.; Chu, Y.-H.; Zheng, H. Visualization of electrode-electrolyte interfaces in LiPF6/EC/DEC electrolyte for lithium ion batteries via in situ TEM. *Nano Lett.* **2014**, *14* (4), 1745–1750.
(18) He, K.; Zhang, S.; Li, J.; Yu, X.; Meng, Q.; Zhu, Y.; Hu, E.; Sun, K.; Yun, H.; Yang, X.-Q. Visualizing non-equilibrium lithiation of spinel oxide via in situ transmission electron microscopy. *Nat. Commun.* **2016**, *7*, 11441.
(19) Zhu, G.-Z.; Prabhudev, S.; Yang, J.; Gabardo, C. M.; Botton, G. A.; Soleymani, L. In situ liquid cell TEM study of morphological evolution and degradation of Pt-Fe nanocatalysts during potential cycling. *J. Phys. Chem. C* **2014**, *118* (38), 22111–22119.
(20) Chen, X.; Noh, K.; Wen, J.; Dillon, S. In situ electrochemical wet cell transmission electron microscopy characterization of solid-liquid interactions between Ni and aqueous NiCl2. *Acta Mater.* **2012**, *60* (1), 192–198.
(21) Sacci, R. L.; Dudney, N. J.; More, K. L.; Parent, L. R.; Arslan, I.; Browning, N. D.; Unocic, R. R. Direct visualization of initial SEI morphology and growth kinetics during lithium deposition by in situ electrochemical transmission electron microscopy. *Chem. Commun.* **2014**, *50* (17), 2104–2107.
(22) Beermann, V.; Holtz, M. E.; Padgett, E.; de Araujo, J. F.; Muller, D. A.; Strasser, P. Real-time imaging of activation and degradation of carbon supported octahedral Pt-Ni alloy fuel cell catalysts at the nanoscale using in situ electrochemical liquid cell STEM. *Energy Environ. Sci.* **2019**, *12* (8), 2476–2485.
(23) Yuan, Y.; Amine, K.; Lu, J.; Shahbazian-Yassar, R. Understanding materials challenges for rechargeable ion batteries with in situ transmission electron microscopy. *Nat. Commun.* **2017**, *8*, 15806.
(24) Woehl, T. J.; Jungjohann, K. L.; Evans, J. E.; Arslan, I.; Ristenpart, W. D.; Browning, N. D. Experimental procedures to mitigate electron beam induced artifacts during in situ fluid imaging of nanomaterials. *Ultramicroscopy* **2013**, *127*, 53–63.

https://dx.doi.org/10.1021/acsomega.0c05829
ACS Omega 2021, 6, 6537–6546

(25) Huang, G.-M.; Huang, C.-W.; Kumar, N.; Huang, C.-Y.; Tseng, T.-Y.; Wu, W.-W. In situ TEM investigation of electron beam-induced ultrafast chemical lithiation for charging. *J. Mater. Chem. A* **2020**, *8* (2), 648−655.
(26) Liu, Y.; Lin, X.-M.; Sun, Y.; Rajh, T. In situ visualization of self-assembly of charged gold nanoparticles. *J. Am. Chem. Soc.* **2013**, *135* (10), 3764−3767.
(27) Chen, Q.; Cho, H.; Manthiram, K.; Yoshida, M.; Ye, X.; Alivisatos, A. P. Interaction potentials of anisotropic nanocrystals from the trajectory sampling of particle motion using in situ liquid phase transmission electron microscopy. *ACS Cent. Sci.* **2015**, *1* (1), 33−39.
(28) Zheng, H.; Mirsaidov, U. M.; Wang, L.-W.; Matsudaira, P. Electron beam manipulation of nanoparticles. *Nano Lett.* **2012**, *12* (11), 5644−5648.
(29) Touve, M. A.; Figg, C. A.; Wright, D. B.; Park, C.; Cantlon, J.; Sumerlin, B. S.; Gianneschi, N. C. Polymerization-induced self-assembly of micelles observed by liquid cell transmission electron microscopy. *ACS Cent. Sci.* **2018**, *4* (5), 543−547.
(30) Klein, K. L.; Anderson, I. M.; De Jonge, N. Transmission electron microscopy with a liquid flow cell. *J. Microsc.* **2011**, *242* (2), 117−123.
(31) Hodnik, N.; Dehm, G.; Mayrhofer, K. J. Importance and challenges of electrochemical in situ liquid cell electron microscopy for energy conversion research. *Acc. Chem. Res.* **2016**, *49* (9), 2015−2022.

https://dx.doi.org/10.1021/acsomega.0c05829
ACS Omega 2021, 6, 6537−6546